DOI: 10.24874/ti.2340.08.26.11

Tribology in Industry

www.tribology.rs

RESEARCH

# Microstructure and Wear Performance of plasma Clad Ti/B4C Composite Coating Developed Over 1020 Carbon Steel

Kamlesh Kumar Singh[a,*], Anil Kumar Das[a]

[a]*Department of Mechanical Engineering, National Institute of Technology Patna, Patna, Bihar, 800005, India.*

Keywords:

*PTA cladding*
*wear rate*
*Ti-B4C ratio*
*B4C ceramic*
*1020 carbon steel*

* Corresponding author:

*Kamlesh Kumar Singh*
*E-mail: kamleshs.ph21.me@nitp.ac.in*

*Received: 20 August 2026*
*Revised: 5 October 2026*
*Accepted: 3 November 2026*

A B S T R A C T

*In this experimental analysis, the effect of variation in Ti/$B_4C$ ratio on surface properties of plasma clad 1020 carbon steel was investigated. The microhardness and wear resistance was reported through Vickers microhardness test and Pin-on-disc Tribo tester respectively. The surface morphology and chemical analysis of coated specimens were analyzed through SEM/EDS and XRD analysis. The XRD analysis of coated tracks confirms the presence of in-situ synthesized $TiB_2$, TiC, $Fe_3C$, $Fe_2Ti$ and $Fe_2B$ in the coatings. The SEM characterization reveals the growth of needle like structures in IC-4 and IC-5 samples. The maximum microhardness reported in IC-5 sample (1158 $HV_{0.1}$)* at 600 µm depth from top *which was 4.106 times higher than the hardness in substrate zone (282 $HV_{0.1}$) and 6.89 times higher than the microhardness of uncoated substrate sample (168 $HV_{0.1}$). The lowest observed mean wear of 3.03 X $10^{-8}$ g $N^{-1}$-$m^{-1}$ was found under the tested conditions in sample IC-5 (50Ti - 50B4C coatings) which was 57.52 times lower than that of the uncoated substrate wear rate (174.3 X $10^{-8}$ g $N^{-1}$-$m^{-1}$ ). The mean friction coefficient reported lowest in IC-1 sample (90Ti-10B4C) which was 0.58 as compared to mean value of uncoated substrate friction (0.72).*

© 2026 Published by Faculty of Engineering

Article in Press

## 1. INTRODUCTION

Metal matrix composites (MMCs) are widely used in marine sector, nuclear reactors and also replacing the conventional materials in aviation sector [1-3]. Due to the difference in properties of matrix and reinforcement phase, MMCs serves both the requirements of strength and wear resistance for the industrial components [2]. PTA cladding, laser assisted coating and thermal spraying of reinforcement particles like Plasma spray and high velocity oxy fuel (HVOF) spray are some of the techniques for developing MMCs [4-6]. Among these, PTA cladding method is less expensive and having higher production rate as compared to other thermal spraying methods [4, 7]. The PTA cladding process uses a non-consumable tungsten electrode. It exhibit many unique advantages such as constricted arc with high energy density, high arc stability and high

melt pool temperature in the range of 8000-10000 $^0$C [2, 8, 9-10]. Also, PTA assisted metallic coatings exhibit improved bond strength than non- metallic coatings [1].

Moreover, coating over mild steel substrate is best suited for marine equipment manufacturing [1, 11]. AISI 1020 carbon steel due to its better tensile strength, best suited in industrial applications [11]. But its low wear resistance limits its applications in harsh service environments and hence there is the need of cladding appears to improve its performance. Sliding wear, salt enriched marine atmosphere, high UV ray's exposure and wear due to hot corrosion cause severe damage to the components and decay its service life [11]. In this context, to minimize the wear rate of substrate materials, carbides are the most widely used reinforcing material [12]. However, the coating of ceramic particles like B4C [13], Boron Nitride [14], WC [15] on mild steel studied by different researchers. Among these, Boron carbide with hardness 3000- 4000 VHN and melting point 2450 $^0$C is widely used to develop hybrid coatings [10,16].

However it is well established fact that direct addition of reinforcing particles over substrate surface bears certain limitations such as poor metallurgical bonding, particles aggregation and crack formation [17]. Therefore, in-situ synthesis of ceramic phases in coatings gained much more attention due to its high thermal stability and interfacial compatibility [17]. Table 1 incorporates the previous research work carried out by different researchers using Ti, B4C particles. From research work enlisted in Table 1, it may be concluded that the addition of Ti and $B_4C$ particles as reinforcement enables the formation of strong metallurgical bond between the coating and the base material and also enhances overall coating performance. Bharti et al. [18] reinforced Ti-$B_4C$-Fe particles over SS304 substrate through TIG cladding route. They reported formation of $TiB_2$, TiC, $B_4C$ and $Fe_3B$ phases in the coatings which increases microhardness up to 820 $HV_{0.1}$ i.e. 4.1 times higher than that of substrate material. Similarly, Li et al. [19] reinforced $CoCrFeNiMnTi_x(B4C)_y$ powder particles through plasma cladding over Q235 steel substrate and achieved microhardness up to 470.8 $HV_{0.2}$ in the coating zone. Han et al. [20] processed Ti, B4C, Mo and HEA powder over 45# steel through laser cladding and achieved significant improvement in hardness of coatings (882.61 HV) whereas Yu et al. [21] utilized Ti, B4C and dr40 particles on the same substrate through laser cladding and achieved average microhardness of 632.66 $HV_{0.3}$ Max. in coatings. Xiang et al. [22] laser clad Ti/B4C particles over Ti6Al4V substrate and achieved average microhardness of 421.2 $HV_{0.5}$ max. in coatings. Cao et al. [23] reported in-situ synthesis of $TiB_2$, TiC and NiAl hard phases in the coatings by PTA cladding of Ti-$B_4C$-Ni-Al reinforcement particles over Q235 steel plates (a grade similar to 1020 carbon steel in composition). It was also concluded by the research team that the role of $B_4C$ was significant in the formation of these hard ceramic phases in the coatings [23]. As B4C weight% increases, it allows more boron and carbon atoms to react with Ti atoms to form TiC, TiB and $TiB_2$ [24]. Li et al. [25] while laser cladding of Ti, B4C and Ni50A particles over H13 steel substrate, reported microhardness up to 659.83 HV0.5 in coatings. Another researcher, Han et al. [13] performed laser cladding over mild steel substrate using $B_4C$, Ti, Cr and Ni particles and achieved microhardness up to 1400 HV0.1 in coatings due to the in-situ formation of TiC, $TiB_2$, $Cr_2Ti$ and $Ni_3Ti$ phases.

**Table 1.** Comparison of present study with previous research work.

| Sl. No. | Substrate | Coating materials | Cladding process | Microhardness value (Average) | Distance between two test points (µm), indentation load (g) and dwell time (s) | Reference |
|---|---|---|---|---|---|---|
| 1 | SS304 | Ti+B4C+Fe | TIG | 820 $HV_{0.1}$ | 100 µm, 100 g, 10 s | [18] |
| 2 | Q235 steel | $CoCrFeNiMn-Ti_x-(B4C)_y$ | Plasma | 470.8 $HV_{0.2}$ | 100 µm, 200 g, 15 s | [19] |
| 3 | 45# steel | HEA powder + Ti+B4C +Mo | Laser | 882.61 $HV_{0.3}$ | 100 µm, 300 g, 8 s. | [20] |
| 4 | 45# steel | Ti, B4C, and dr40 | laser | 632.66 $HV_{0.3}$ | 100 µm, 300 g | [21] |
| 5 | Ti 6Al4V | Ti+B4C | Laser | 421.2 $HV_{0.5}$ | 100 µm, 500 g, 10 s | [22] |
| **6** | **1020 steel** | **Ti+B4C** | **Plasma** | **955 $HV_{0.1}$** | **(100 µm - first 10 indents, 200 µm- next 7 indents), load 100 g, dwell- 10 s** | **Present study** |

Article in Press

The above literature discussed direct comparison of Ti/B4C coatings produced by different cladding methods which gives a better insight for understanding coating performance. Moreover, Literature reviews shows that laser cladding, PTA cladding and TIG arc assisted cladding over mild steel substrate were very popular among research community. Balbande et al. [26] deposited tantalum and graphite powders over AISI 8620 steel plate by TIG cladding with in-situ tantalum carbide formation and achieved increased microhardness up to 630- 670 HV0.1. In an another investigation, Chen et al. [14] in order to improve hardness of Q235 steel substrate, utilized SS 316L and hexagonal boron nitride (h-BN) through coaxial powder feeding mechanism in laser cladding. The hardness maximum in coatings was found 438 HV. They concluded that low laser power and high scan speeds produced defects leading to lowering of microhardness value of coatings. Another researcher, Guo et al. [27] interestingly combined semi-solid paste green coating and co-axial powder feeding technique in laser cladding over low carbon steel plates. Ni and Cu powders mixed and deposited in form of paste over substrate and then Ti-6Al-4V particles were supplied through powder feeding mechanism while laser processing. Friction coefficient reported in the range of 0.18- 0.32 for claddings during wear test. Wear volume loss up to 0.03 $mm^3$ in coatings reported as compared to that of substrate (0.17 $mm^3$) which shows developed coatings were highly wear resistant. Dharavathu et al. [28] concluded that at high speed laser cladding, COF decreases. The COF of coatings lie in the range of 0.2 to 0.4 during wear test. Wang et al. [29] and Mirshekari et al. [30] performed high entropy alloy coating over low carbon steel substrate and achieved hard surfaces in both cases. Wang et al. [29] deposited Fe-Cr-Mo-C-B-Y alloy powder over 1020 steel pipe through laser-powder feed mechanism and observed martensitic structure in coating zone. Mirshekari et al. [30] changed the way of depositing reinforcing particles over mild steel substrate. They used flux cored wire filled with HEA powder [AlCoCrFeNiTi0.5] fed manually while TIG arcing and achieved hardness of 550- 600 HV. In another research, Gol et al. [31] studied the effect of varying boron concentration from 10 to 30 % in a multi-component alloy powder reinforced TIG cladding over low carbon steel substrate. The coating results in very high hardness reaching up to 1811 $HV_{0.3}$ (30% boron concentration) compared to boron free coatings (834 $HV_{0.3}$). The friction coefficient value for coatings was comparatively low and in the range of 0.6- 0.7 as compared to substrate (0.85). Biswas et al. [15] studied the effect of varying current from 70- 110 A during TIG cladding of WC-Co-Cr particles over low carbon steel substrate and concluded that lower current value leads to low friction coefficient of coatings during wear test (0.4 at 70 A) and comparatively high friction coefficient (0.5 and 0.6) at 90 and 110 A respectively. The maximum hardness also achieved at low current value of 70 A which was 1480 $HV_{0.1}$. Li et al. [32] performed PTA cladding over Q235 steel substrate and observed friction coefficient of the coatings in the range of 0.55- 0.35 and hardness 800- 1400 $HV_{0.2}$. This increased hardness and lower friction coefficient was due to the formation of (Ti, Mo)C hard phases in the coating zone. In an another investigation, Yang et al. [33] deposited 50, 60 and 70 % overlap laser-clads over low carbon steel substrate and concluded that overlap reduces the wear rate of coatings. The wear rate of 0.0149 x $10^{-5}$ $mm^3N^{-1}$-$m^{-1}$ to 0.0114 x $10^{-5}$ $mm^3N^{-1}$-$m^{-1}$ observed in 50 to 70 % overlapped tracks as compared to substrate wear rate (1.96 x$10^{-5}$ $mm^3N^{-1}$-$m^{-1}$) which depicts that deposition of overlap tracks always beneficial for producing wear resistant coatings. Kumar et al. [34] deposited double ceramic coating layer over 1020 carbon steel using 50%TiO2- 50%TiB2 particles and checked the effect of varying current. It was noted that maximum microhardness of 568 $HV_{0.05}$ achieved at lowest value of current input (110 Amp), other parameters remaining constant.

Based upon the literature survey, Ti and B4C as coating materials were selected due to their attractive mechanical and tribo-properties which has been shown by a significant no. of research articles. The novelty of this research lies in the fact that a wide range of varying composition of Ti/B4C ratio effects on wear performance of coatings has been studied. Also, due to the unique arc characteristics of plasma as a heat source, it was used for depositing Ti/B4C particles over 1020 steel substrate to enhance the coating performance. Therefore, this study is targeted in order to find optimum Ti- B4C weight% composition along with plasma-clad approach to increase wear resistance of 1020 carbon steel substrate.

## 2. EXPERIMENTAL PROCEDURES

### 2.1 Materials and methods

Six substrate plates of AISI 1020 carbon steel (supplied by Parshwamani Metals, Mumbai, India) with sample size 49 x 70 x 6 $mm^3$ were cut and

Article in Press

designated as P1 to P6. Then, the plates were abraded with #220 SiC emery paper and cleaned with acetone to remove surface contaminants. B4C powder <10 µm size, density 2.52 g/cm$^3$, 98% purity and Ti powder 1-5 µm size, density 4.506 g/cm$^3$ and 98 % purity level (both supplied by Sigma Aldrich) were used as cladding materials.

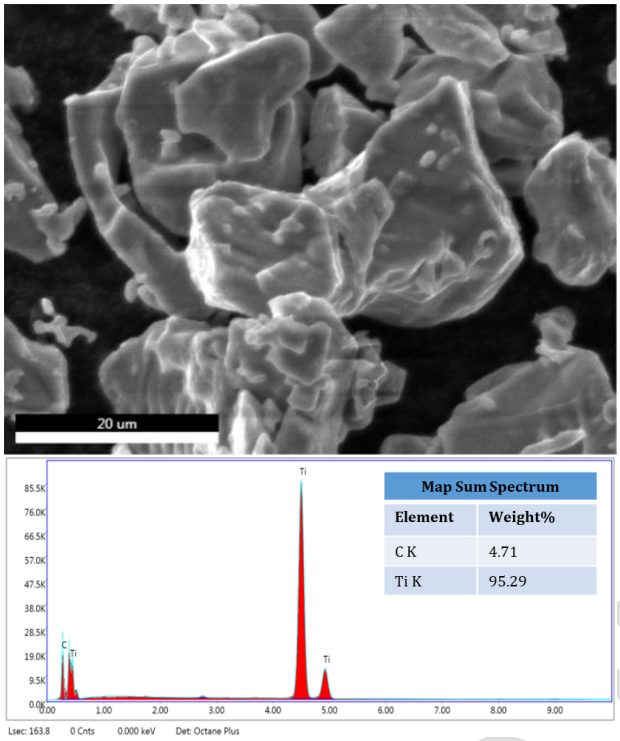



**Fig. 1.** SEM image of Ti powder with EDS result.

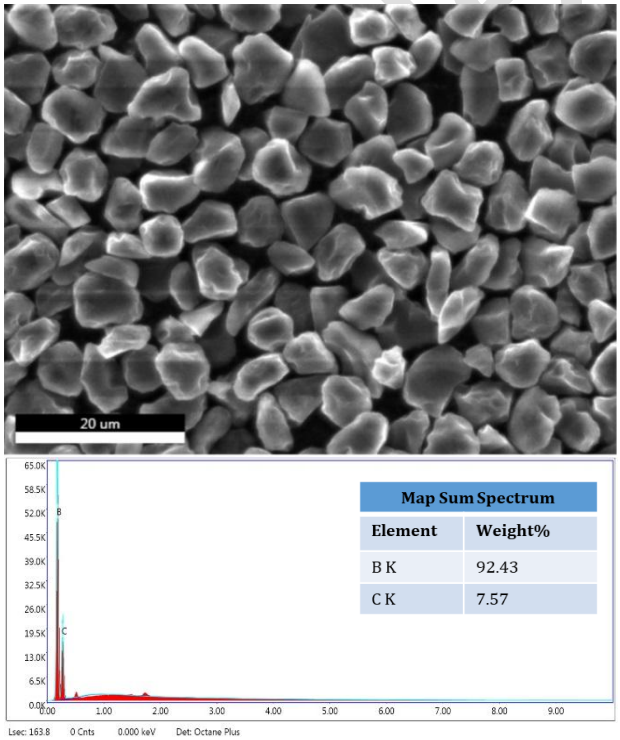



**Fig. 2.** SEM image of B4C particles with EDS result.

Powder particle morphology of Ti and B4C particles obtained through SEM/EDS depicts that the powder particles were irregularly shaped and were evenly distributed which is presented in figures (1) and (2) respectively. A mixture of 90Ti-10B4C, 80Ti-20B4C, 70Ti-30B4C, 60Ti-40B4C, 50Ti-50B4C and 40Ti-60B4C used for preparing green coating to deposit over six substrate plates. Mass of Ti and B4C powder were used as per their weight % composition. For 300 µm green coating thickness, the calculated powder mass for Ti were 3.87, 3.21, 2.63, 2.11, 1.66 and 1.26 gram respectively for six compositions whereas amount of powder mass for B4C were 0.43, 0.80, 1.13, 1.41, 1.66 and 1.88 gram respectively. 5% PVA solution was added as binder material along with Ti and B4C to make semi solid paste. The paste spread evenly on the entire surface of 1020 carbon steel substrate by maintaining a green coating thickness of 300 µm. After that, this primarily bond coat substrate samples were cured for 48 hours at room temperature to remove moisture from the pre-coat layer and to make it completely dry and ready for PTA processing.

## 2.2 PTA cladding technique

PTA-250 cladding machine (supplied by Technocrats Plasma Systems Pvt. Ltd, Mumbai, India) with integrated 3 axis automated movement facility for plasma torch (controlled by in-built PLC circuit) was used for depositing single layer tracks. The schematic diagram of the PTA cladding set up is shown in Figure 3(a). In PTA- welding, the transferred arc is generated by connecting substrate and plasma torch to the positive and negative terminal respectively.

Argon gas was used as both Plasma and shielding gas whose flow rates were 6 and 10 l/min respectively. The flow rates of shielding and plasma gas was continuously monitored during the entire cladding operation. The process parameters selected for PTA cladding deposition is mentioned in Table 2. Four tracks deposited at four different current levels i.e. 75, 80, 85 and 90 Amps on each plates P1-P6. The value of plasma cladding process parameters for voltage, arc gap and scan speed were 15V, 4 mm and 100 mm/min respectively selected by conducting trial runs while coating deposition. Specimens were

Article in Press

selected from the tracks by visual examination. The images of coatings deposited and selected tracks for characterization is shown in figure 3(b). Melting of substrate plate due to overheating reported in coatings deposited at 90 Amps in plates P-2 and P-4. Among all, tracks deposited at 80 Amps reported with uniform bead and without any visual defects and therefore these tracks were separated from each plate and designated as IC-1, IC-2, IC-3, IC-4, IC-5, IC-6 and were considered for further metallographic examinations.

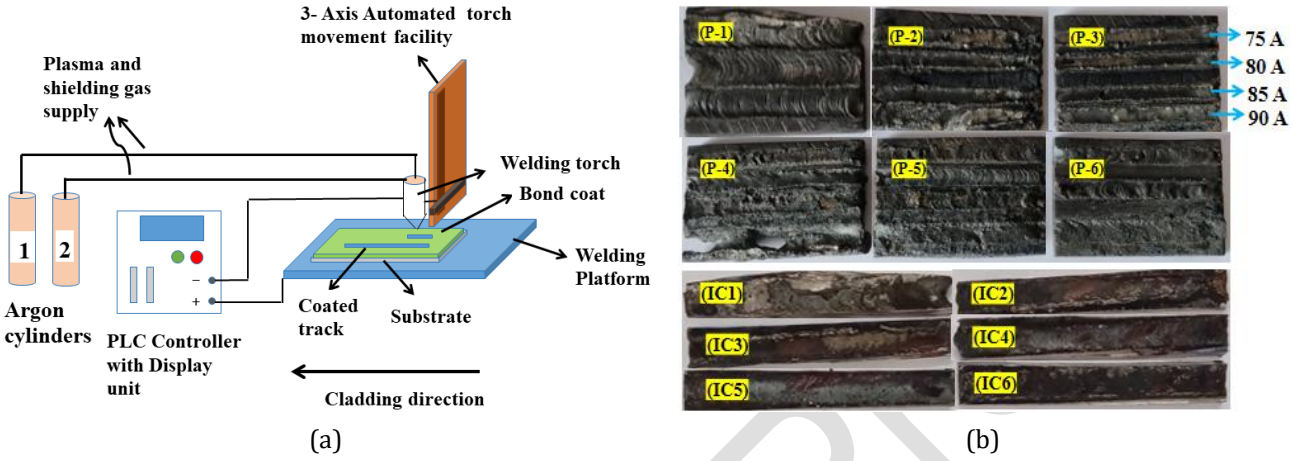



**Fig. 3.** (a) Schematic diagram of Plasma Transferred Arc Cladding process, (b) Images of coatings deposited and selected tracks for characterization.

**Table 2.** PTA cladding process parameters along with Ti/B4C ratio.

| Sl. No. | Sample No. | Ti/B4C ratio | Reinforcing particles (Weight %) | | PTA parameters | | |
|---|---|---|---|---|---|---|---|
| | | | Ti | B4C | Current (Amps) | Voltage (V) | Scan Speed (mm/min.) |
| 1 | IC-1 | 90Ti - 10B4C | 90 | 10 | 80 | 15 | 100 |
| 2 | IC-2 | 80Ti - 20B4C | 80 | 20 | 80 | 15 | 100 |
| 3 | IC-3 | 70Ti - 30B4C | 70 | 30 | 80 | 15 | 100 |
| 4 | IC-4 | 60Ti - 40B4C | 60 | 40 | 80 | 15 | 100 |
| 5 | IC-5 | 50Ti - 50B4C | 50 | 50 | 80 | 15 | 100 |
| 6 | IC-6 | 40Ti - 60B4C | 40 | 60 | 80 | 15 | 100 |

## 2.3 Surface morphology and XRD analysis

The coated tracks were sectioned using abrasive cutter in the transverse direction of the track deposited with dimension 10 x 10 x 6 $mm^3$ for SEM analysis to visualize surface morphology. Then, the sectioned samples were abraded at the lateral crosss-section using 400- 5000 grit emery paper followed by gentle rubbing on velvet cloth with diamond paste of 0.5- 1 µm [supplied by Chennai Metco] to remove the scratch marks and to get a mirror finish. Then, the samples were etched using 5% Nital solution. Flowchart of sample preparation strategy for SEM analyze is shown in figure 4. The characterization of surface morphology of samples were carried out in Nova NanoSEM 450 scanning electron microscopy facility in back scattered diffraction (BSD) mode of imaging and the presence of chemical elements were verified by energy dispersive spectroscopy.

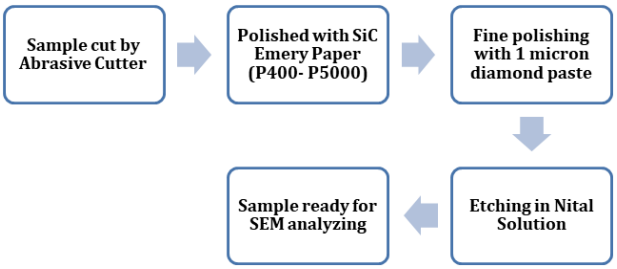



**Fig. 4.** Flowchart showing sample preparation strategy for SEM.

Structural characterizations of coatings were performed using a Rigaku mini flex x-ray diffraction (XRD) machine. The XRD samples for

analyze required no surface treatment. X-ray diffraction (XRD) test parameters were Cu-Kα radiation with wavelength (λ=1.5406 $A^0$), scan range (2θ) from $20^o$ to $80^o$, sampling step 0.02 and 2s per point scan time. The main objective behind this characterization was to recognize the in-situ synthesized phases in the coatings.

### 2.4 Microhardness and wear analysis

The microhardness at lateral section of samples was evaluated through Vickers microhardness testing machine (Model: UHL VMHT, made by Walter UHL, Germany). For Vickers microhardness, the coatings sectioned in the form of 10 x 10 x 6 $mm^3$ blocks and abraded with 220- 3000 grit SiC emery paper and then cleaned with acetone. 17 indentations were recorded from top of coating along the depth at lateral cross section of samples. First 10 indentations from top to bottom recorded along depth at 100 µm distance between two adjacent test points. Thereafter, 200 µm distances kept for remaining 7 indentations along the same vertical line of indentation. This variation in distance between two test points after 10 indents was kept keeping in view the average coating depth of the samples IC-1 to IC-6. Microhardness parameters were indentation load 100 g, dwell time 10s and magnification 50X.

Wear test of the samples was performed on pin on disc tribo tester (TE-165-SPOD, supplied by Magnum Engineers). Fig. 5 shows the top view of the wear test condition. All the wear test samples were sectioned in dimension of 8 x 8 x 6 $mm^3$. Each sample undergone gentle rubbing with 400 grit size SiC emery paper to make the coated sliding surfaces even throughout followed by cleaning with acetone. The wear test carried out with EN31 hardened steel disc rotating in counter clockwise direction in relation to stationary, rectangular, Ti/B4C top pins. Each coated pin's top surface on which coating was deposited, kept in upside down position while performing wear test with EN31 counter-body. Before performing wear test, the top surface of EN31 counterface abraded gently with 400 and 600 grit size SiC emery paper followed by cleaning with acetone. This was done to remove circumferencial scratch marks of wear tracks from the counterbody. Hardness 697 HV and initial surface roughness (Ra) 0.32 µm reported for EN31 counterface. Reconditioned counterface track was used for performing each wear test. The wear test parameters are listed in Table 3. The wear test parameters were normal load 10 N, rotational speed of EN31 Steel counterface 200 rpm, track radius 35 mm and distance traveled 439.82 m. Test duration for each sample was 10 min. Ambient temperature $31^0$C and 80 % relative humidity recorded at the time of wear test. Three specimens cut from each (IC-1 to IC-6) deposited track and therefore 18 specimens in total prepared for wear test of coatings. The average microhardness of all three samples (for each powder formulation) was determined to assess the variation within that coating. Average microhardness for coatings was calculated considering the microhardness associated with all indents made in coating zone [20].

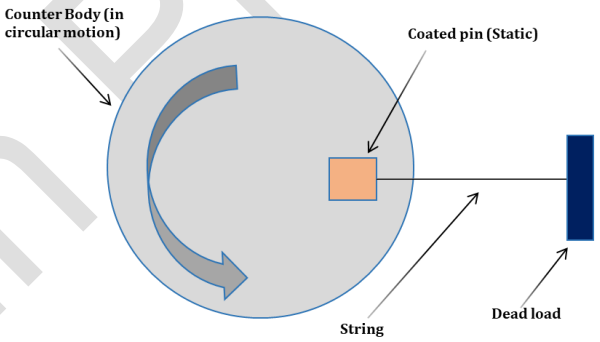



**Fig. 5.** Top view of Pin-on-disc wear test environment.

**Table 3.** wear test parameters.

| Parameters | Values |
|---|---|
| Speed of EN31 Steel disc | 200 rpm |
| Normal load | 10 N |
| test duration | 10 min. |
| Track radius | 35 mm |
| Sliding distance | 439.82 m |

The weights of the coated pins were recorded before and after the wear test using electronic weighing machine (Manufactured by Mettler Toledo, Precision 0.1 mg) to estimate the mass loss due to wear of pins. Acetone was used to clean the samples before weighing. Specific wear rate for each sample was calculated thereof using eqn. 1. After completion of wear test, morphology of the surfaces tested were examined through SEM followed by subsequent chemical analyzing through EDS.

$$\text{Wear rate } (\text{g N}^{-1}\text{m}^{-1}) = \frac{\text{Weight loss of coated pin (g)}}{\text{Normal load (N) X Sliding distance (m)}} \quad (1)$$

Article in Press

## 3. RESULT AND DISCUSSION

### 3.1 XRD analysis

The XRD spectra of the top surface of the coated samples IC-1, IC-2, IC-3, IC-4, IC-5 and IC-6 are displayed in figure 6. The in-situ synthesized phase constituents present in the coatings were identified by utilizing Xpert High Score Plus software and the XRD spectra was plotted with the help of OriginPro 2026 software. Multiple hard ceramic phases were formed due to in-situ reaction between Ti-B4C reinforcing particles and elements present in 1020 carbon steel substrate. The presence of $TiB_2$, TiC, $Fe_3C$, $Fe_2Ti$ and $Fe_2B$ phases were reported in the coatings. Similar evolved phases were observed by Bharti et al. [18]. Table 4 shows a list of phases identified in XRD analysis along with crystal structure, peak positions and orientation of grains shown by miller indices as per JCPDS No. All IC-1 to IC-6 samples shows several crystalline phases with varying peak strengths. $TiB_2$ and $Fe_2Ti$ phases have hexagonal crystal structure. Whereas Fe3C, TiC and B4C exhibit orthorhombic, cubic and rhombohedral crystal structure respectively as per XRD investigation of coatings. $Fe_2B$ phase reported with tetragonal crystal structure at $69.20^0$ (2θ) as per JCPDS No. 01-072-1301. Fe3C phases identified at $26.5^0$ (2θ) as per JCPDS reference pattern no. 01-085-0871. TiB2 phase at peak positions $34.14^0$ and $56.98^0$ identified as per JCPDS No. 01-075-1045. The minimum presence of iron based ceramic phases in the IC-5 sample leads to tentative interpretation that there may be very less thermal driven Marangoni flow of Fe from substrate content in the weld pool i.e. the capillary flow of Fe in the weld pool in upward direction was minimal. The presence of higher proportion of TiC, and TiB2 in IC-5 sample (50% Ti- 50% B4C) was found. The higher proportion of unreacted B4C in samples IC-1, IC-2 and IC-3 observed at peak positions $34.88^0$ and $53.4^0$. The amount of unreacted B4C is minimal in samples IC-4, IC-5 and IC-6 which represent that major portion of B4C dissociated during cladding operation and formed new phases like TiB2 and TiC.

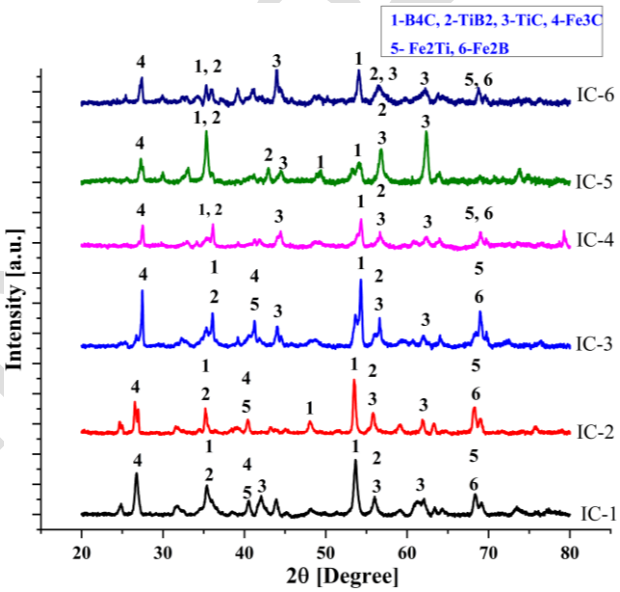



**Fig. 6.** XRD spectrum of coated samples (IC-1 to IC-6).

**Table 4.** Phases identified in XRD analysis.

| Phase | Crystal structure | Peaks (2θ) | Miller Indices (hkl) | JCPDS No. |
|---|---|---|---|---|
| B4C | Rhombohedral | 34.88, 53.40 | (104), (205) | 01-075-0424 |
| TiB2 | Hexagonal | 34.14, 56.98 | (100), (002) | 01-075-1045 |
| TiC | Cubic | 41.80, 60.61 | (200), (220) | 01-089-3828 |
| Fe3C | Orthorhombic | 26.5 | (002) | 01-085-0871 |
| Fe2Ti | Hexagonal | 40.78, 68.8 | (103), (301) | 03-065-0602 |
| Fe2B | Tetragonal | 69.20 | (103) | 01-072-1301 |

### 3.2 Surface morphology of coatings

Bead geometry indicating the depth of coatings is shown in figure 7. Samples IC-2, IC-3 and IC-6 reported lower coating depth with values 1.64 mm, 1.42 mm and 1.29 mm respectively. Whereas higher coating depths reported in samples IC-1, IC-4 and IC-5 with values 2.46 mm, 2.02 mm and 2.06 mm respectively. The higher coating depth indicates more diffusion of the substrate material. The measurement of coating depth was done with ImageJ software along the vertical line at the mid-section of coated specimens. Lot of porosity reported in sample IC-6 as evident from figure 7 (f).

Article in Press

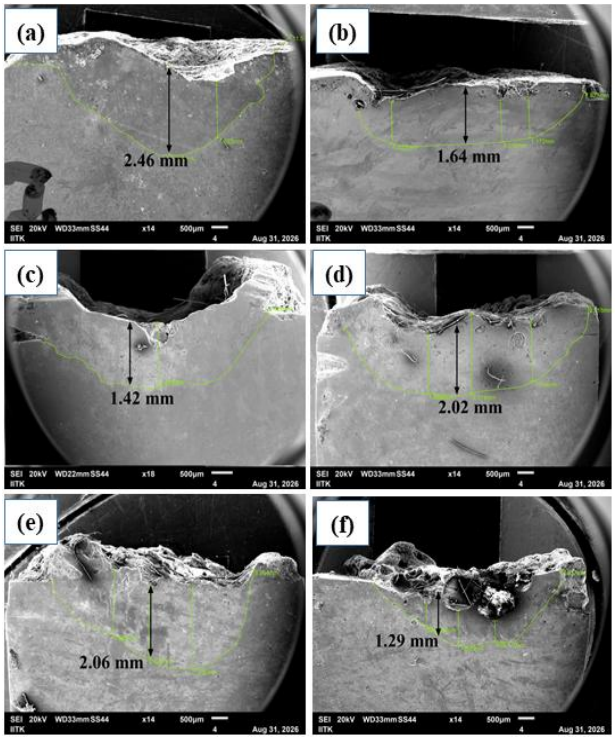



**Fig. 7.** Bead geometry of coatings IC-1 to IC-6 (a-f).

Surface morphology of the coated samples recorded through FESEM facility (Provided by Advance Imaging Lab, IIT Kanpur). Figure 8 and 9 differentiates the coating zone and the substrate zone with interface line. From figure 8 (a) and (b) in sample IC-1 and IC-6, cracks formation along the interface zone was clearly identified. It is obvious that interface boundary line observes the highest thermal gradient separating the substrate and the coating zone which may be a reason for the formation of crack along this separation line and the same was discussed by Liu et al. [35]. Figure 8(b) illustrates crack generation during solidification process in coated sample IC-6 with composition 40Ti- 60B4C, which also indicates that high weight % of ceramic particle reinforcement in the coating may also be one of the reason behind the formation of this crack. The same micro cracks were observed by Li et al. when addition of TiC exceeds 40 wt% [36]. Figure 8 (a) shows that presence of large number of voids and blow holes in the coating zone in sample IC-1 (90Ti- 10B4C weight % composition) which as a result lowered the performance of the IC-1 sample coating. Higher amount of metallic powder reinforcement in sample IC-1 (90Ti- 10B4C) and higher amount of ceramic particle reinforcement in sample IC-6 (40Ti- 60B4C) may also be one of the reason for the formation of cracks along the interface line in sample IC-1 and IC-6. This indicates weak metallurgical bond formation between the substrate and coated layer in both the coated samples IC-1 and IC-6. The formation of needle like structures and lamellar grain growth can also be viewed in FESEM images of sample IC-4 and IC-5 through the figure 9(b), 9(c) respectively.

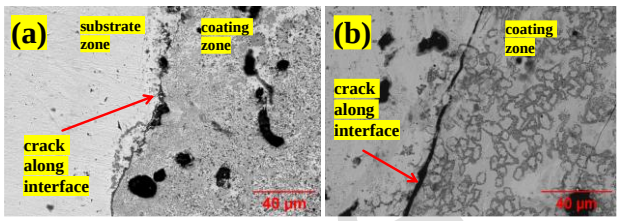



**Fig. 8.** FESEM images of samples (a) IC-1 (b) IC-6 indicating crack along interface.

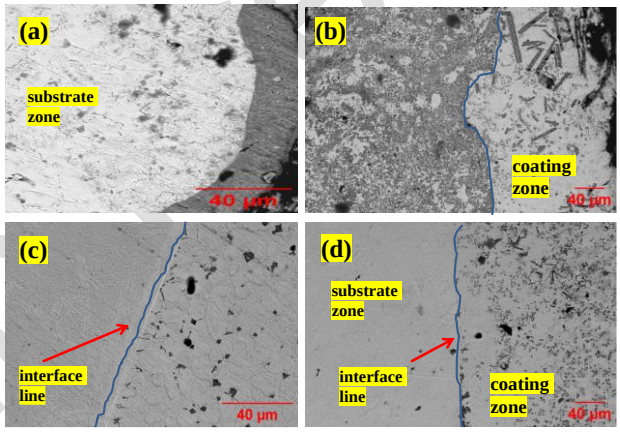



**Fig. 9.** Surface morphology at lateral section of samples IC-2 to IC-5 (a -d).

FESEM images at high magnification level for all coated samples IC-1 to IC-6 showing the microstructure is displayed in figure 10. Surface morphology of IC-4 and IC-5 shows the formation of needle like structures developed during solidification after cladding. Moreover, through high magnification FESEM image 10 (f) in sample IC-6, crack formation can also be observed clearly along the interface separation line between substrate zone and coating zone.

EDX spectrum of sample IC-5 acquired in the coating zone and its element map is shown in figure 11. Through elemental map, sample IC-5 (50%Ti-50%B4C coatings) reports the presence of boron, carbon, titanium and iron elements in the coating zone in amounts of 1.07, 1.78, 10.65 and 86.5 weight % respectively. The richness of iron and titanium elements in the coating was also confirmed by visualizing the map sum spectrum of 50%Ti-50% B4C coating.

Article in Press

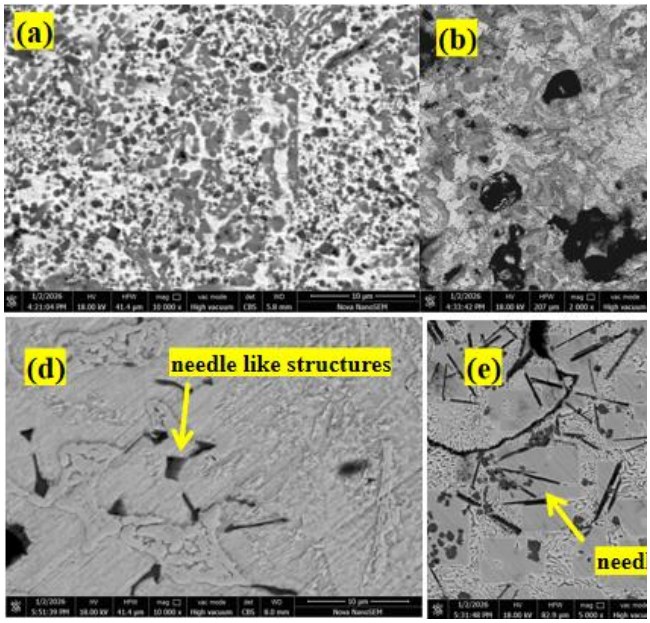



**Fig. 10.** High magnifications SEM image of coatings IC-1 to IC-6 (a-f).

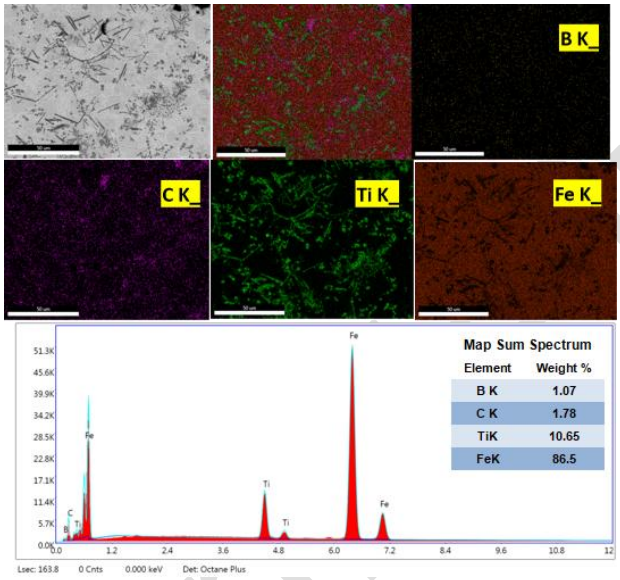
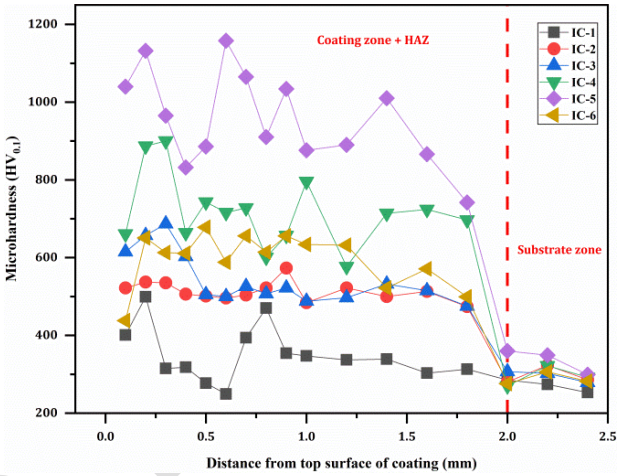



**Fig. 11.** Surface morphology with element map of sample IC-5.

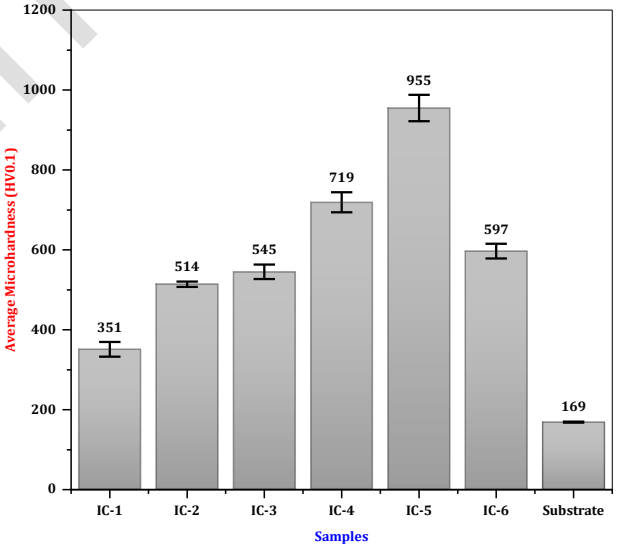
The higher Fe content in coating zone of sample IC-5 may be due to the presence of higher amount of Fe ~99.08% in 1020 carbon steel. It is also evident that due to substrate dilution during PTA cladding, the Fe wt% reduced to 86.5% in sample IC-5 and still remains higher in content as compared to boron, carbon and titanium.

### 3.3 Hardness measurements

The Vicker's microhardness values for different coated samples and uncoated substrate is displayed in Figure 12 (a). Figure 12 (b) shows the average microhardness values for IC-1 to IC-6 sample and uncoated substrate. The reported average hardness includes measurements from the heat-affected zone and the coating zone. The variation from mean value is represented with error bar. The error bar in Figure 12 (b) shows the standard error of the measured microhardness values with respect to mean value within a sample.




(a)




(b)

**Fig. 12.** (a) Microhardness along coating depth of the samples (IC-1 to IC-6), (b) Average microhardness (including heat-affected zone and coating zone) of samples IC-1 to IC-6 and uncoated substrate.

Sample IC-5 with composition 50Ti-50B4C gives the highest and best microhardness values among all the coated samples. This was directly linked to production of hard and wear resistant coating as increased hardness value indicates that indentation was difficult through the surface along the depth of coating for 50Ti-

50B4C. The highest microhardness value of 1158 HV0.1 was reported at 600 µm depth from top in IC-5 sample. This was the coating maximum value of hardness and 6.65 times higher than that of uncoated substrate hardness (174 HV0.1 Max.).The hardness comparison is shown in figure 13(a) which depicts that sample IC-5 will offer maximum resistance to indentation as compared to substrate leading to superior material performance. The 90Ti-10B4C coatings show lowest microhardness. The substrate zone of coatings bears very low microhardness value as the indenter indents more into the substrate. The diamond shaped indent made by the indenter in the substrate zone is comparatively bigger in size as compared to the indent made in the coating zone observed in figure 13 (b) captured at same magnification while hardness measurements.

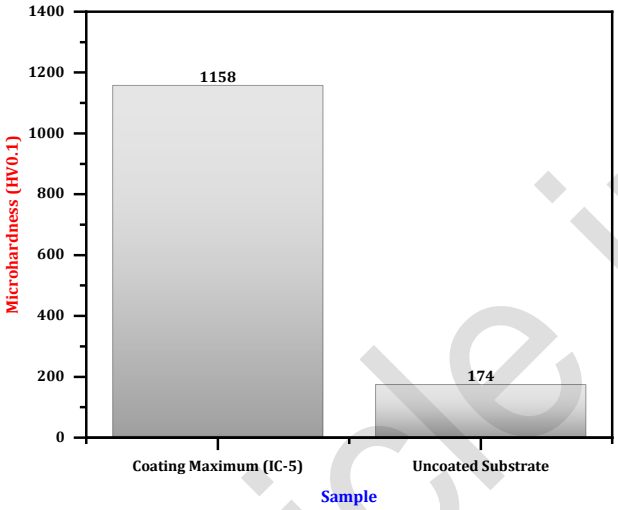



**Fig. 13**. (a) Hardness comparison (coating) $_{Max.}$ and (uncoated substrate) $_{Max}$, (b) Optical images of indentation in coating and substrate zone of a sample.

### 3.4 Analysis of wear test results

Three trials for each powder formulation carried out and its average value was calculated for specific wear rate and co-efficient of friction estimation. Table 5 shows the values of wear rate along with means, standard deviations and standard errors. In fig. 14, wear rate of samples IC-1 to IC-6 and uncoated substrate is shown along with error bar. The error bar in figure 14 shows standard error i.e variability of reported wear with respect to mean value of a sample for three replications. From fig. 14, it is evident that the specific wear rate of sample IC-5 was the lowest (3.03 X $10^{-8}$ g $N^{-1}$-$m^{-1}$ ) that means the coating deposited with 50%Ti- 50%B4C undergone lowest mass loss due to wear and exhibit optimum wear resistance. Wear rate of 16.67 X $10^{-8}$ g $N^{-1}$-$m^{-1}$ stands for sample IC-1 (90Ti -10B4C coatings) which was highest wear loss among the coatings deposited. The wear rate for sample IC-2 and IC-3 was 9.85 X $10^{-8}$ g $N^{-1}$-$m^{-1}$ and 3.79 X $10^{-8}$ g $N^{-1}$-$m^{-1}$ respectively. Wear rate of samples IC-4 and IC-6 were 7.58 X $10^{-8}$ g $N^{-1}$-$m^{-1}$ and 8.34 X $10^{-8}$ g $N^{-1}$-$m^{-1}$ respectively. The specific wear rate for uncoated sample reported was 174.3 X $10^{-8}$ g $N^{-1}$-$m^{-1}$ which shows that uncoated steel substrate exhibit very low wear resistance. Wear response was non-monotonic for the 6 compositions IC-1 to IC-6 as identified from measured wear values (figure 14). Wear decreased from IC-1 to IC-3, increased in IC-4, then decreased to its lowest level in IC-5, and then increased once more in IC-6. In case of IC-5 wear was found to be lowest, nearly 81.82% less than IC-1. This non-monotonic wear behavior may be due to differences in microstructure and phase distribution of coatings. The lowest observed mean wear under the tested conditions and the highest average hardness was observed for IC-5 sample and it imply that IC-5 has better capability of resisting surface deformation and material removal.

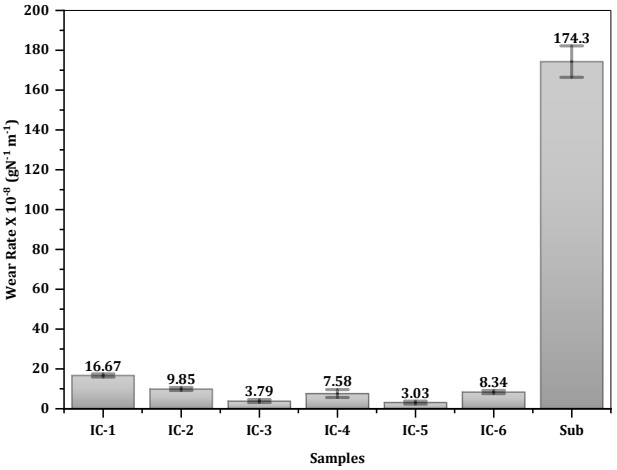



**Fig. 14.** Wear rate of samples IC-1 to IC-6 and uncoated substrate with error bar.

Article in Press

**Table 5.** Wear rate of samples (IC-1 to IC-6) and uncoated substrate for three trials.

| Wear rate X $10^{-8}$ g $N^{-1}$-$m^{-1}$ | | | | | | | |
|---|---|---|---|---|---|---|---|
| **Sample** | **IC-1** | **IC-2** | **IC-3** | **IC-4** | **IC-5** | **IC-6** | **Substrate** |
| **Trial 1** | 15.915 | 11.368 | 2.27 | 6.82 | 2.27 | 9.094 | 188.71 |
| **Trial 2** | 15.91 | 9.094 | 4.547 | 4.547 | 4.547 | 6.82 | 172.79 |
| **Trial 3** | 18.18 | 9.094 | 4.547 | 11.368 | 2.27 | 9.094 | 161.42 |
| **Mean** | **16.668** | **9.852** | **3.788** | **7.578** | **3.029** | **8.336** | **174.307** |
| **Standard Deviation** | 1.309144 | 1.3128945 | 1.31462656 | 3.47315596 | 1.31462656 | 1.312895 | 13.708072 |
| **Standard Error** | 0.755835 | 0.758 | 0.759 | 2.00522753 | 0.759 | 0.758 | 7.914359 |

The coefficient of friction vs. time graph is shown in fig. 15. The coefficient of friction value for uncoated 1020 substrate was above 0.8 with mean value 0.72. The coefficient of friction vs. time plot for uncoated substrate (Figure 15) reports very high fluctuations during the maximum wear test duration. The value of coefficient of friction in the first 20 seconds during test conduct (running-in time) was lower for all the test samples and as the contact between the counter body and the samples established fully, the value of coefficient of friction along Y-axis attains the maximum peak and becomes almost static during the remaining test duration.

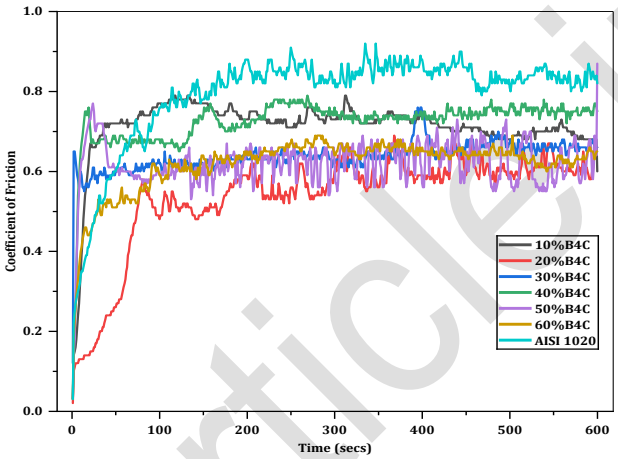



**Fig. 15.** Coefficient of friction vs. Time curve for IC-1 to IC-6 samples and uncoated substrate.

In figure 16, the mean coefficient of friction values were mapped along the Y-axis with error bar and samples with different compositions along X- axis. The error bar represents the standard error of the mean value of friction coefficient for three trials each composition. The mean friction coefficient values were 0.58, 0.66, 0.7, 0.75, 0.74 and 0.6 for coatings IC-1 to IC-6 respectively. Among coatings, IC-1 has the lowest reported mean friction coefficient i.e. 0.58, whereas IC-5 has the lowest reported wear i.e. 3.03 X $10^{-8}$ g $N^{-1}$-$m^{-1}$. This implies that the composition with the best wear resistance may not also provide the lowest friction.

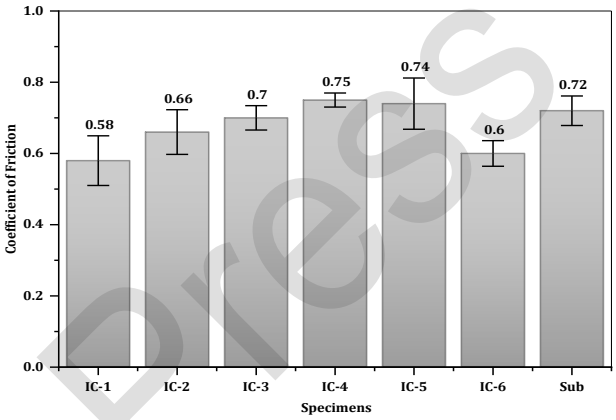



**Fig. 16.** Mean coefficient of friction plot of samples IC-1 to IC-6 and uncoated substrate.

### 3.5 Surface morphology of wear tracks

The FESEM images of wear out samples (IC-1 to IC-6) and uncoated substrate is shown in fig. 17. After visual examination of the FESEM images, the presence of wear debris, deep grooves, shallow grooves, pits, and signs of plastic deformation reported across different coated samples. Deep grooves creation and particle coming out in the form of debris reported in sample IC-2 (80%Ti-20%$B_4C$). The FESEM images of IC-3 sample reports formation of pits and presence of wear debris on the worn out surface. Figure 18 shows surface morphology of IC-3 and IC-5 worn surfaces using FESEM images, recorded at 200 µm length scale and 500X magnifications. Figure 19 shows the EDX elemental map of IC-5 (50% Ti- 50% B4C) which indicates the presence of boron, carbon, silicon, titanium and iron elements in the coating. The sample damage severity due to wear in IC-5 was lesser than that of the substrate and it may be due to the increased surface hardness and lower wear rate. The severe wear in IC-6 leads to increase in wear rate substantially as compared to IC-5 sample. Huge material loss due to wear in uncoated substrate sample reported which may be due to its lower surface hardness. Since the wear rate was minimal in IC-3 and IC-5 samples, it needs direct comparison of these two wear surfaces.

Article in Press

From Figure 18, it is evident that IC-3 has undergone wear damage along the sliding direction whereas damage in IC-5 sample surface was comparatively minimal along the sliding direction. The wear pattern inclined to the sliding direction in IC-5 and it may be due to entrapped wear particles and hard asperities abrasion behavior. The hard asperities abrasion produces fluctuation in friction co-efficient graph as evident from figure 15.

The wear loss from a material surface follows some wear mechanisms. Abrasive wear happens when grooves follow the sliding direction. It happened in IC-2 and IC-3 sample as reported from figure 17 (b) and (c). Formation of pits reported in uncoated substrate as evident from Figure 17 (g) which indicates delamination wear was predominant mechanism during dry sliding wear of the sample against EN31 counterbody.

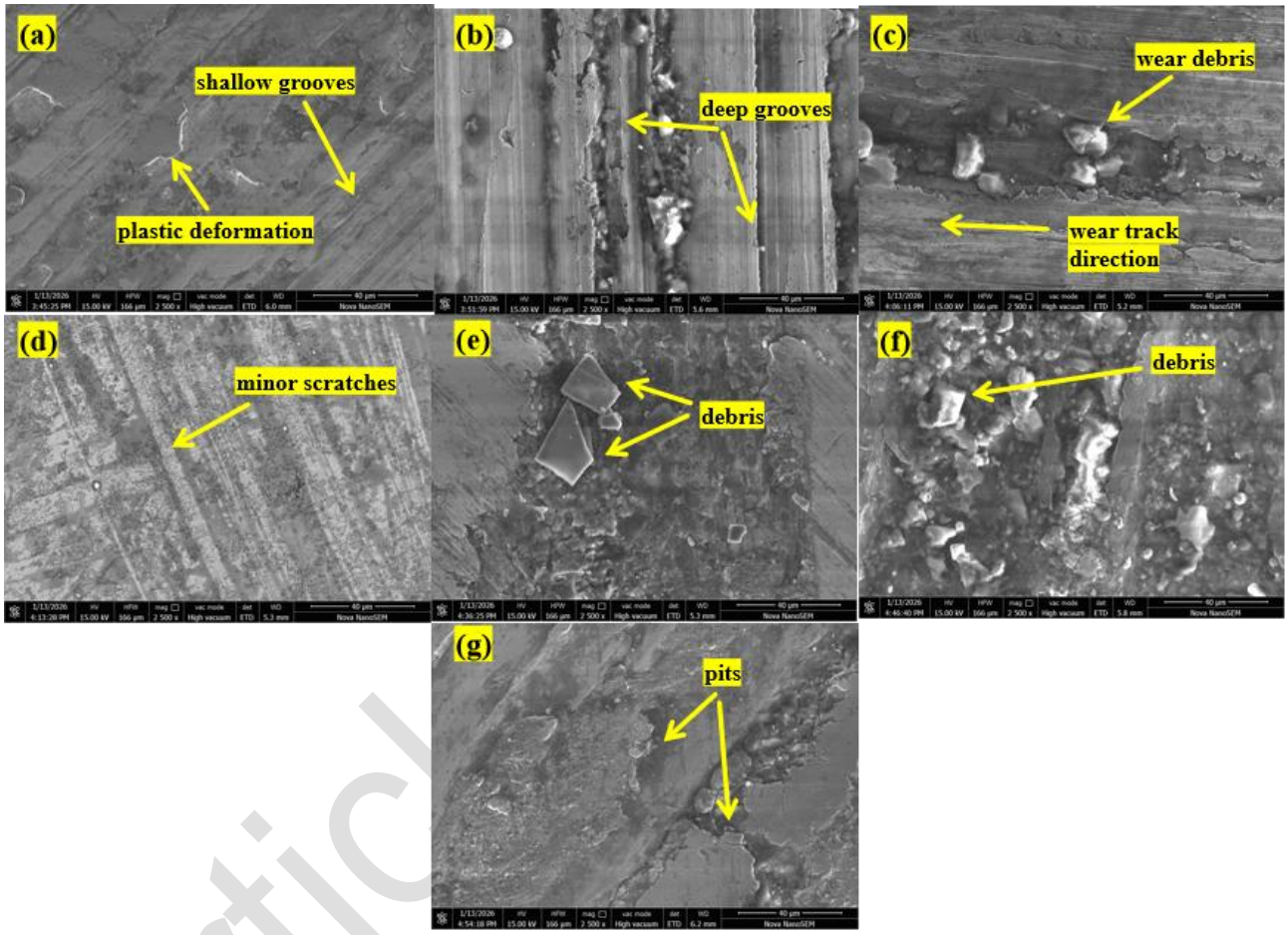



**Fig. 17.** SEM images of worn surface (a-f) - (IC-1 to IC-6) and (g)- uncoated substrate.

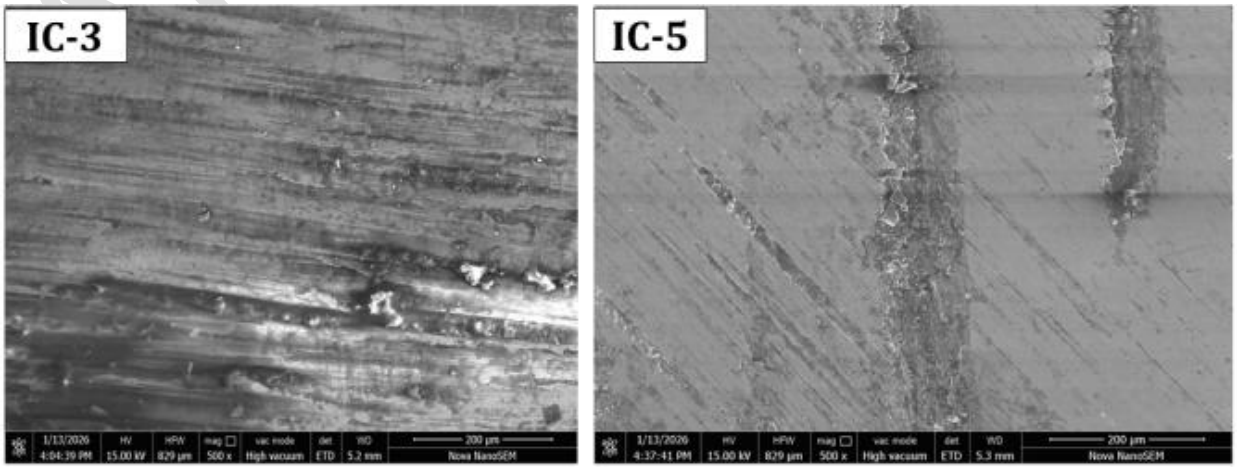



**Fig. 18.** SEM image of IC-3 and IC-5 wear out samples showing sliding direction.

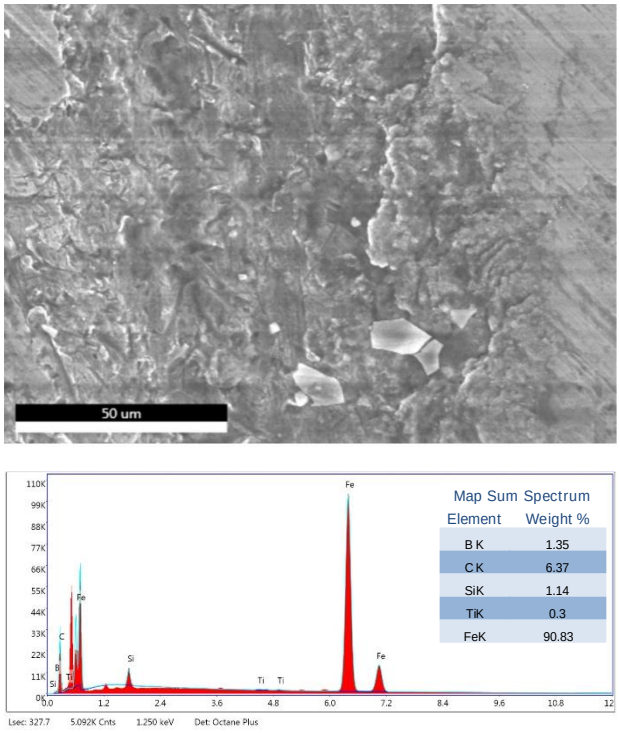



**Fig. 19.** Worn surface EDS study of sample IC-5.

## 4. CONCLUSIONS

Wear resistant Ti- B4C reinforced composite coating produced successfully over 1020 carbon steel substrate by PTA processing route. Therefore, the following conclusions were formulated from this experimental investigation.

1. The 20%, 30%, 40% and 50% B4C additions as per weight ratio in Ti/B4C feed mixture, results in coating formation without any defect with formation of $TiB_2$, TiC, $Fe_3C$, $Fe_2Ti$ and $Fe_2B$ phases in the coatings.
2. The sample IC-5 (50%Ti-50%B4C) reported maximum average microhardness 955 $HV_{0.1}$ and lowest mean wear rate under the tested conditions (3.03 X 10-8 g N-1-m$^{-1}$).
3. The crack along interface line observed in FESEM images in sample IC-1 (90%Ti-10%B4C) and IC-6 (40%Ti-60%B4C) is an indication that at 80A current input, 10 and 60 weight% B4C addition in Ti/B4C feed mixture leads to failure of coatings along interface line.
4. The coated sample IC-5 deposited with 50%Ti-50%B4C feed mixture exhibit 6.65 times greater microhardness value (1158 $HV_{0.1}$ maximum at 600 µm depth from top surface) in the coating zone as compared to uncoated 1020 steel (174 $HV_{0.1}$) which reflects substantial increase in surface strength of 1020 carbon steel.
5. Sample IC-5 (50Ti-50B4C coatings) bears lowest observed mean wear rate of 3.03 X $10^{-8}$ g $N^{-1}$-$m^{-1}$ under the tested conditions which was 57.52 times lower than that of uncoated substrate wear test coupon (174.3x$10^{-8}$g$N^{-1}$-$m^{-1}$).

## Acknowledgement

The Authors want to thank Advance Imaging Lab, Indian Institute of Technology Kanpur for providing FESEM facility. The Authors also want to extent their gratitude to DST-SERB, Govt. of India, for providing research grant for PTA cladding and Pin-on-disc Tribotester at NIT Patna (DST-SERB research grant File No: EEQ/2020/000272).

## REFERENCES

[1] K. Hu, Y. Tian, X. Jiang, H. Yu, and D. Sun, "Microstructure regulation and performance of titanium alloy coating with Ni interlayer on the surface of mild steel by laser cladding," *Surface and Coatings Technology*, vol. 487, Art. no. 130939, May 2024, doi: 10.1016/j.surfcoat.2024.130939.

[2] C. Zhang, L. Zhang, S. Zhang, S. Li, J. Li, Y. Zhou, and Z. Xie, "Structural evolution and tribological properties of WC Particles-Strengthened Nickel-Based cladding layers," *Journal of Materials Engineering and Performance*, vol. 34, no. 14, pp. 13807–13820, Oct. 2024, doi: 10.1007/s11665-024-10177-3.

[3] X. Cao, L. Wang, R. He, L. Zhou, and C. Lin, "Characterization of Fe-Based layers deposited by laminar plasma cladding on Low-Carbon steel," *Journal of Thermal Spray Technology*, vol. 32, no. 7, pp. 2104–2111, Jul. 2023, doi: 10.1007/s11666-023-01634-x.

[4] M. Ulutan, K. Kiliçay, O. N. Çelik, and U. Er, "Microstructure and wear behaviour of plasma transferred arc (PTA)-deposited FeCrC composite coatings on AISI 5115 steel," *Journal of Materials Processing Technology*, vol. 236, pp. 26–34, May 2016, doi: 10.1016/j.jmatprotec.2016.04.032.

[5] J. R. Da Cruz, C. E. B. Marino, and A. S. C. M. D' Oliveira, "Corrosion resistance of FeCrMnSiB austenitic stainless steels processed by plasma transferred arc," *Journal of Materials*

Article in Press

*Engineering and Performance*, vol. 34, no. 12, pp. 10865–10875, Aug. 2024, doi: 10.1007/s11665-024-09893-7.

[6] R. Soundararajan, K. Kaviyarasan, A. Sathish kumar, and S. Sivasankaran, "Evaluating the metallurgical and corrosion characteristics of HVOF-sprayed Ni and Ni-TiB2 coatings on duplex stainless steel," *Ceramics International*, vol. 51, no. 6, pp. 7636–7650, Dec. 2024, doi: 10.1016/j.ceramint.2024.12.202.

[7] Y. Zhou, Y. Liu, Z. Huang, S. Wang, Z. Yue, W. Zhang, and C. Dong, "Microstructure, wear, and corrosion performance of spherical cast tungsten carbide reinforced stainless steel-based composites manufactured by plasma transferred arc techniques," *Vacuum*, vol. 233, Art. no. 114003, Dec. 2024, doi: 10.1016/j.vacuum.2024.114003.

[8] X. Shi, Y. Liu, M. Zhang, and Z. Sun, "Dual-constricted plasma arc cladding of Inconel 625 alloy: arc characteristics, microstructure, and corrosion resistance," *Journal of Materials Science Materials in Engineering*, vol. 20, no. 1, Mar. 2025, doi: 10.1186/s40712-025-00262-3.

[9] L. Chen, M. Li, S. Wang, Z. Guo, B. Liang, J. Xue and Z. Guo, "Microstructure and corrosion resistance of Ni-Al coating prepared by plasma transferred arc technology," *Journal of Materials Engineering and Performance*, vol. 33, no. 4, pp. 1596–1614, Mar. 2023, doi: 10.1007/s11665-023-08084-0.

[10] G. X. Zhou, T. Zhao, R. Wang, C. H. Zhang, L. C. Wu, S. Zhang, and J. Chen, "Study on microstructure and cavitation resistance of Fe-Based and Ni-Based alloy coatings by plasma transfer arc welding," *Journal of Materials Engineering and Performance*, vol. 34, no. 18, pp. 19881–19894, Feb. 2025, doi: 10.1007/s11665-025-10705-9.

[11] W. Gao, S. C. Wang, K. K. Hu, X. Z. Jiang, H. Y. Yu, and D. B. Sun, "Effect of laser cladding speed on microstructure and properties of titanium alloy coating on low carbon steel," *Surface and Coatings Technology*, vol. 451, Art. no. 129029, Nov. 2022, doi: 10.1016/j.surfcoat.2022.129029.

[12] L. H. R. Apolinário, E. A. Torres, H. R. Araújo, A. De Albuquerque Vicente, and T. F. De Abreu Santos, "Effect of laser cladding parameters in NbC reinforced 316L austenitic stainless steel composite depositions on a mild steel," *The International Journal of Advanced Manufacturing Technology*, vol. 122, no. 7–8, pp. 3095–3113, Sep. 2022, doi: 10.1007/s00170-022-10067-9.

[13] T. Han, M. Xiao, J. Zhang, X. Feng, and Y. Shen, "Laser cladding composite coating on mild steel using Ni–Cr–Ti–B4C powder," *Surface Engineering*, vol. 36, no. 12, pp. 1278–1284, Oct. 2018, doi: 10.1080/02670844.2018.1534926.

[14] Y. Chen, Y. Xu, T. Li, J. Du, L. Guo, and K. Hu, "Fabrication and characterization of self-lubricating anti-wear 316L stainless steel/h-BN composite coatings on Q235 substrate via laser cladding," *Optics & Laser Technology*, vol. 180, Art. no. 111564, Aug. 2024, doi: 10.1016/j.optlastec.2024.111564

[15] K. Biswas and C. K. Sahoo, "The performance evaluation of WC/Co-Cr coating for developing hard, wear, and corrosion resistance surface using TIG arc source," *International Journal of Refractory Metals and Hard Materials*, vol. 128, Art. no. 106983, Nov. 2024, doi: 10.1016/j.ijrmhm.2024.106983.

[16] K. K. Singh and A. K. Das, "Recent developments in Plasma Transferred Arc assisted metal matrix composite coating: A review," *IOP Conference Series Materials Science and Engineering*, vol. 1334, no. 1, Art. no. 012012, Sep. 2025, doi: 10.1088/1757-899X/1334/1/012012.

[17] R. Wang, S. Ye, P. Cheng, Z. Xie, Y. Wang, Y. Zhang, G. Li, W. Wu, X. Lu, "Microstructure and wear resistance of in-situ TiC reinforced Stellite 6 coating using PTA cladding," *Journal of Materials Research and Technology*, vol. 27, pp. 2656–2669, Oct. 2023, doi: 10.1016/j.jmrt.2023.10.053.

[18] A. Bharti, S. M. Pandey, and A. K. Keshri, "Investigation of microstructural and mechanical properties of tungsten inert gas Weld-Cladded Ti-B4C-Fe layer on AISI 304SS," *Journal of Materials Engineering and Performance*, vol. 35, no. 12, pp. 11519–11532, Aug. 2025, doi: 10.1007/s11665-025-11695-4.

[19] S. Li, P. Zhang, X. Xue, Y. Sun, Z. Liu, S. Du, and H. Liu, "Reaction-Induced Microstructure Evolution and Properties of Plasma-Cladded $CoCrFeNiMnTi_x(B4C)_y$ High-Entropy Alloy Composite Coatings with In-Situ Carbide-Boride Networks," *Journal of Thermal Spray Technology*, vol. 35, no. 7, pp. 3153–3172, Aug. 2026, doi: 10.1007/s11666-026-02314-2.

[20] P. Han, J. Geng, G. Wang, Y. Duan, Z. Wu, and Y. Li, "Co-optimizing wear and corrosion resistance via composition design: The role of B4C in $(Fe50Mn30Co10Cr10)_{0.75-x}Ti_{0.15}(B4C)_xMo_{0.1}$ laser-cladded composite coatings," *Intermetallics*, vol. 197, Art. no. 109373, Jun. 2026, doi: 10.1016/j.intermet.2026.109373.

[21] J. Yu, J. Chen, and H. Ho, "Effect of laser cladding Ti/B4C/dr40-based composite coatings for the surface strengthening of shaft part," *Optics &*

Article in Press

*Laser Technology*, vol. 157, Art. no. 108721, Oct. 2022, doi: 10.1016/j.optlastec.2022.108721.

[22] D. Xiang, D. Wang, S. Wang, L. Yan, and Y. Chen, "Analysis and optimization of laser cladding Ti-B4C composite coatings based on the interaction and GABP-NSGAII algorithm," *Surface and Coatings Technology*, vol. 493, Art. no. 131186, Jul. 2024, doi: 10.1016/j.surfcoat.2024.131186.

[23] L. Cao, Y. Xia, H. Cui, Q. Li, B. Zhu, and Q. Wang, "Microstructural characteristics of TiB2–TiC–NiAl composite coatings via Plasma Cladding Process," *Surface Engineering*, vol. 35, no. 11, pp. 997–1002, May 2019, doi: 10.1080/02670844.2019.1611002.

[24] W. Wang, K. Zhang, F. Wu, and W. Liu, "Effect of B4C content on the microstructure and corrosion properties of In-situ reinforced TI-6AL-4V coatings by laser directed energy deposition technology," *Journal of Materials Engineering and Performance,* vol. 35, no. 21, pp. 20812–20819, Feb. 2026, doi: 10.1007/s11665-026-13430-z.

[25] Z.-W. Li, T. Lin, L. Li, C. N. Jing, Y. M. Tu, N. N. Liu, and X. Yang, "Effect of Ti content on microstructure evolution and properties of Ni50A-B4C coatings," *Ceramics International*, vol. 51, no. 23, pp. 40108–40121, Jun. 2025, doi: 10.1016/j.ceramint.2025.06.245.

[26] S. Balbande, S. Rai, G. Agarwal, and S. Das, "Effect of TIG-arcing speed on the microstructure vis-à-vis mechanical behaviour of surface modified low carbon steel," *Wear*, vol. 570, Art. no. 205924, Feb. 2025, doi: 10.1016/j.wear.2025.205924.

[27] W. Guo, H. Zhang, Y. Li, and Z. Li, "Fabrication of high-performance Ti–6Al–4V laser cladding layer on low carbon steel using Ni/Cu as interlayers," *Materials Chemistry and Physics*, vol. 345, Art. no. 131280, Jul. 2025, doi: 10.1016/j.matchemphys.2025.131280.

[28] R. Dharavathu, K. Shetty, and G. Muvvala, "A study on laser cladding of Stellite 6 by conventional and high-speed laser cladding process," *Surface and Coatings Technology*, vol. 515, Art. no. 132623, Aug. 2025, doi: 10.1016/j.surfcoat.2025.132623.

[29] H. Wang, Y. Cheng, Y. Wan, N. Jeyaprakash, Y. Wang, K. Ma, and J. Wang, "Influence of scanning speed on microstructure and corrosion resistance of Fe-based amorphous coatings by high-speed laser cladding," *Surface and Coatings Technology*, vol. 479, Art. no. 130449, Jan. 2024, doi: 10.1016/j.surfcoat.2024.130449.

[30] A. Mirshekari, G. R. Khayati, and S. Arjmand, "TIG-clad Fe-based AlCoCrNiTi0.5 high-entropy alloy coating on low-carbon steel: microstructure, microhardness, and corrosion resistance," *Surface and Coatings Technology*, vol. 517, Art. no. 132826, Oct. 2025, doi: 10.1016/j.surfcoat.2025.132826.

[31] Y. Gol and B. Kilinç, "Effect of boron concentration in the Fe-Cr-Mo-(B,C) hardfacing alloys on the microstructure and mechanical properties," *Journal of Materials Engineering and Performance*, vol. 34, no. 14, pp. 14325–14336, Oct. 2024, doi: 10.1007/s11665-024-10123-3.

[32] M. Li, D. Ma, J. Chi, S. Wang, X. Song and F. Chen, "Effect of in situ (Ti,Mo)C on the microstructure and properties of FeMoSi/ γ-(Ni,Fe) composite coatings by PTA cladding," *Materials Today Communications*, vol. 49, Art. no. 113785, Sep. 2025, doi: 10.1016/j.mtcomm.2025.113785.

[33] Z. Q. Yang, H. M. Kuo, H. C. Chiang, and C. H. Hung, "Enhanced wear resistance of low carbon steel by depositing iron-chromium alloy coating using high-power laser cladding," The International *Journal of Advanced Manufacturing Technology*, vol. 137, no. 3–4, pp. 1133–1147, Feb. 2025, doi: 10.1007/s00170-025-15271-x.

[34] S. Kumar and A. K. Das, "Evaluation of mechanical properties of TiB2 -TiO2 ceramic composite coating on AISI 1020 mild steel by TIG cladding," *Engineering Research Express*, vol. 4, no. 1, Art. no. 015034, Mar. 2022, doi: 10.1088/2631-8695/ac5ae7.

[35] D. Liu, D. He, H. Li, N. Li, L. Ma, H. Li, and J. Yu, "Multi-ceramic phases synergistically reinforced titanium matrix composite coating deposited by laser cladding: Effect of B4C content on the microstructure and wear properties," *Surface and Coatings Technology*, vol. 496, Art. no. 131648, Dec. 2024, doi: 10.1016/j.surfcoat.2024.131648.

[36] J. Li, C. Chen, T. Squartini, and Q. He, "A study on wear resistance and microcrack of the Ti3Al/TiAl + TiC ceramic layer deposited by laser cladding on Ti–6Al–4V alloy," *Applied Surface Science*, vol. 257, no. 5, pp. 1550–1555, Sep. 2010, doi: 10.1016/j.apsusc.2010.08.094.

Article in Press